International Journal For Recent Developments in Science & Technology
2581-4575
Crossref
A Peer Reviewed Research Journal

A Reliable Solution for Lung Cancer Detection

[1]A Vasavi Sujatha, [2]G. Laxmi, [3]M.Mary, [4]S. Akshitha

[1] Assistant Professor, Department of Information Technology, Bhoj Reddy Engineering College for Women, Vinay Nagar, Hyderabad

[2,3,4] Student, Department of Information Technology, Bhoj Reddy Engineering College for Women, Vinay Nagar, Hyderabad

Abstract

The exact lung cancer identification is a critical problem that has attracted the researchers' attention. The practice of multiview single image and segmentation has been widely used for the last 2 years to improve the identification of lung cancer disease. The utilization of machine learning (ML) and deep learning (DL) techniques can significantly expedite the process of cancer detection and stage classification, enabling researchers to study a larger number of patients in a shorter time frame and at a reduced cost applying the image segmentation approach herein, the multiresolution rigid registration mechanism is applied to enhance the segmentation further. Techniques like principle component averaging and discrete wavelet transform are verified for the image fusion development. To review the performance of the suggested technique, the image database resource initiative-based lungs image database consortium is tested in this paper which includes 4,682 computed tomography scan images of 61 patients with nodules sizes from 3 to 30 mm. According to the study finding, the outperformed results of our model are obtained in terms of feature mutual information, and peak signal-to-noise ratio, which were recorded at 0.80 and 19.25, respectively. Moreover, the detection and stages of cancer (STG-1, STG-2, STG-3, and STG-4) of lung nodules are also assessed by using the ResNet-18 convolutional neural network classifier. With only 1.8 FP/scan, the achieved accuracy and sensitivity for detection are 98.2% and 96.4%, respectively. The study's findings show that our proposed strategy outperforms existing models significantly. Therefore, the proposed models have the potential to be implemented in clinical settings to provide support to doctors in the early diagnosis of cancer, while minimizing the occurrence of false positives in scans.

1. Introduction

Lung cancer is a common lethal illness that takes estimated 422 lives worldwide everyday [1]. People over age 50 mostly develop cancer, so the number of lung cancer patients increases everyday [2]. Since lung cancer is difficult to detect relative to other diseases, it is considered one of the leading causes of death. The primary cause of failure is the small size of the lesion, which is referred to as a nodule. Cancer cell size is small in the beginning stage, but it grows and becomes malignant after a certain period. Therefore, controlling the disease at an early stage has become important. If cancer is detected early, the survival rate can be improved [3]. Recently, computer vision researchers have developed high-tech networks that automatically spot and identify healthy and tumor areas [4].

Machine learning (ML) is indeed a branch of artificial intelligence (AI) that has evolved from the study of pattern recognition and cognitive learning principles. It focuses on creating algorithms and models that have the ability to learn and adapt from extensive datasets. By leveraging this data, ML models can make predictions and decisions based on past experiences and patterns. ML algorithms are designed to analyze and extract meaningful information from large datasets. They can identify patterns, correlations, and trends that may not be apparent to humans. Through a process of training, where the model learns from labeled examples or historical data, ML algorithms can generalize and make pre-dictions on new unseen data. The applications of ML are vast and diverse, ranging from image and speech recognition to natural language processing, recommendation systems, fraud detection, and autonomous vehicles, among many others. ML has become a critical tool in extracting insights, automating tasks, and enhancing decision-making processes across vari-ous industries. [5]. Deep learning (DL) is an advanced form of ML that excels in tasks such as feature extraction, object detection, voice recognition, and other domains that involve complex data processing [6]. It utilizes deep neural networks with multiple layers to extract and learn intricate patterns from data. DL has demonstrated exceptional capabilities in various fields and has been known to achieve remarkable efficiency, sometimes surpassing human performance.

Transfer learning (TL) is a technique in ML and DL that involves utilizing preexisting knowledge gained from one task to improve the performance of another related task. TL is particularly useful when there is limited labeled data available for the target task. It can be applied in two ways: as a baseline algorithm, used to train the image dataset and evaluate performance; and as a feature extractor, where fea-tures are extracted from image datasets and used with ML or DL algorithms to assess the performance. Ensemble learning, on the other hand, involves combining multiple purposefully developed learning models to address problems such as classification [7]. It is a ML technique that aims to enhance predictive accuracy by integrating multiple models. Addi-tionally, it is a prominent area of research for improving base classification models [8].

A number of papers have been published on a distinct strategy for detecting cancer [6, 9–11].

One imaging modality is inadequate to give the morpho-logical and functional data needed to diagnose the normal and diseased structures in medical imaging. To provide expanded medical knowledge that cannot be seen with a single imaging modality, multiview medical imaging requires the use of two or more images. Multiview diagnostic imaging improves the identification of lesions, cancerous cells, non-cancerous cells, and tumors [12]. Multiview image registra-tion and fusion can create a final image that contains the most details. Registration and fusion procedures are used to resolve this constraint to diagnose certain diseases more reli-ably [13]. Image registration works in the lines of geometrical dimensions of both images and matches their level of inten-sity. After image fusion, the next step is to overlays both images without removing significant clinical information. The resulting merged image will provide anatomical and functional information. Medical image fusion is the process of combining various single-modality medical images to bet-ter understand the morphological structure and metabolic state of lesions and provide a more accurate disease diagno-sis. A common medical image fusion combines single-mode different computed tomography (CT) images in slices. CT imaging examines how distinct parts of the human body absorb X-rays. It can capture the human skeleton and has cancer using advanced ML techniques. This approach involves the development of an efficient ML classification model, utili-zation of feature extraction methods, exploration of multiview medical image registration, fusion algorithms, and evaluation using performance indicators. The research aims to contribute to the field by providing a robust and accurate solution for lung cancer detection, ultimately improving patient out-comes and advancing medical applications in this domain.

This study has achieved several significant accomplish-ments, which can be summarized as follows:

(1) First, we propose the multiresolution rigid registra-tion (MRR) technique, which is applied in a distinc-tive manner by employing identical sizes and resolutions for feature extraction of lung CT image.
(2) Second, we have developed an effective technique discrete wavelet transform (DWT) as well as princi-pal component averaging for the detection of lung cancer, which involves the automated extraction of features from CT images without requiring any user intervention.
(3) Last, we conduct an analysis of our proposed model by employing the ResNet-18 model for the purpose of diagnosing lung nodules and performing stage classi-fication, there by contributing to the new ML-based applications.

The remaining sections of the paper are organized as follows: Section 2 provides a comprehensive literature review on the subject being investigated; Section 3 presents a detailed description of the dataset used and an analysis of the methodology employed in our study; Section 4 is dedi-cated to the discussion of the experimental results obtained; finally, Section 5 presents the conclusion of our study and outline potential future directions for the research.

2. Related Work

This section provides a comprehensive review of different image fusion methods specifically designed for multiview images.

2.1. Lung Cancer Using CAD Approach. Silva et al. [15] pro-posed a CAD approach, as described in their publication, which was based on the U-Net and ResNet-34 architectures. The method was applied to four different cross-cohort data-sets. To evaluate the performance of their approach, the authors utilized the dice similarity coefficient (DSC). The DSC is a commonly used metric in medical image segmen-tation tasks and measures the overlap between the predicted and ground truth segmentations, with a value ranging from 0 to 1. A DSC value of 1 indicates a perfect overlap between the predicted and ground truth segmentations. According to the findings reported by Silva et al. [15], the CAD approach achieved a mean DSC value exceeding 0.93 across the four different cross-cohort datasets. This suggests that the method performed well in accurately segmenting and delineating structures of interest in the medical images. The method was reviewed by two radiation experts who identified certain

limitations, particularly in the case of consolidation. How-ever, the developed system achieved an accuracy of over 99.3% and an F-score of 99.2%. The study employed four performance metrics to evaluate the disease. Additionally, the system was evaluated using two DL tools on three datasets.

In the work by Alsheikhy et al. [16], a manual process machine was developed for the detection of lung cancer. The process involved utilizing numerous CT images and a Gabor filter. The dataset used consisted of 1,800 images, out of which 900 were images of children diagnosed with lung can-cer. Each image had a size of 200 × 200 pixels, and the data-set was collected from the IMBA Home Database. However, the study did not mention any specific performance metric or provide results. This CAD system achieves an average accuracy of 99.42%, with a maximum accuracy of 99.61%. Furthermore, the system achieves impressive results for other considered performance metrics, with recall, precision, and F-score reaching 99.76%, 99.88%, and 99.82%, respectively.

2.2. Lung Cancer Using CNN Approach. An update CNN model was introduced by Li and Zhao [17] to estimate the volume of the ventriculus sinister using MR images for mul-tiview fusion. A method for using fuzing images that uses translation-invariant wavelets and cascaded principle com-ponent averaging (PCA) was proposed by Benjamin and Jayasree [18]. According to the experiments, the fusion method outperforms the visual and quantitative assessment frameworks. An adaptive dictionary learning method for multiview medical image fusion was proposed by Aishwarya and Thangammal [19]. For dictionary learning, useful infor-mation blocks were separated by removing zero data blocks and using multi-scale feature to approximate the remaining image patches. This reduced the amount of computing while simultaneously producing a high-quality image [19].

Similarly, Faruqui et al. [20] applied a deep-CNN-based model designed to enhance the accuracy of CAD of lung cancer. It combines CT-scan images and wearable sensor-based medical IoT (MIoT) data to improve the diagnostic capabilities. The unique 22-layer CNN architecture of Lung-Net extracts features from both data sources, resulting in high accuracy of 96.81% and a low-false positive (FP) rate of 3.35% for classifying lung cancer into five classes. It out-performs similar CNN-based classifiers. LungNet also clas-sifies stage-1 and stage-2 lung cancers into subclasses with 91.6% accuracy and a FP rate of 7.25%. Operating from a centralized server, LungNet has been trained on a balanced dataset of 525,000 images. Its high accuracy, low-FP rate, and substage classification make it a promising solution for auto-matic lung cancer diagnosis systems.

Nasser and Abu-Naser [21] introduced an artificial neu-ral network (ANN) model designed for detecting lung cancer in the human body. The model utilized a range of symptoms as inputs to diagnose the disease. To train and validate the model, the survey lung cancer dataset was utilized, resulting in an accuracy of approximately 96.67% after more than 1,418,000 learning cycles. However, the approach proposed in the current article surpasses the aforementioned accuracy, achieving over 99% accuracy in a reduced number of learn-ing cycles, demonstrating its superiority. Furthermore, com-pared to the model presented in [20], the execution time of the approach described in this article is shorter. The CAD system developed in this study demonstrated high perfor-mance, with accuracy, recall, precision, and F-score reaching 99.42%, 99.76%, 99.88%, and 99.82%, respectively. The research-ers customized and encapsulated two DL tools, namely VGG-19 and LSTMs, to achieve these results.

2.3. Lung Cancer Detection Using Algorithm. Shimazaki et al. [22] developed and validated a DL model to detect lung cancer on chest radiographs using the algorithmic method. The training dataset consisted of 629 radiographs containing 652 nodules/masses, while the test dataset included 151 radiographs with 159 nodules/masses. In the independent test dataset, the model achieved a sensitivity of 0.73 and a mean false positive indication per image (mFPI) of 0.13. However, the sensitivity of the model was lower for lung cancers that overlapped with blind spots compared to non-overlapped locations. The dice coefficient, which measures the similarity between predicted and ground truth masks, for malignant lesions had an average value of 0.52. This indicates that the model's performance in accurately delineating malignant lesions was moderate. Despite these limitations, the DL-based model demonstrated promise in detecting lung cancers on chest radiographs with low-FP rates, as indicated by the low MFPI. Further research and improvements may be required to enhance the model's sensitivity, particularly for lung cancers overlapping with blind spots, and to improve the dice coefficient for malignant lesions.

Hasan and Al Kabir [23] developed algorithms for deter-mining the spread of cancer in a patient's lungs. These algo-rithms employed image processing techniques and statistical learning methods. The evaluation was conducted on a data-set comprising 198 images sourced from the Kaggle plat-form, achieving an accuracy of approximately 72.2%. In comparison, the approach examined in this article achieves a significantly higher accuracy of 99.42%. Furthermore, the proposed algorithm in this study attains impressive results with recall, precision, and F-score reaching 99.76%, 99.88%, and 99.82%, respectively. These outcomes demonstrate the superiority of the method presented in this study.

Furthermore, Bhatia et al. [24] implemented an algorithm for detecting lung cancer using deep residual learning on CT-scan images. The authors employed U-Net and ResNet mod-els to extract features and identify potential

cancer-prone regions. Multiple classifiers, including XG boost, random for-est (RF), and individual predictions, were used to predict cancer. The algorithm achieved an accuracy of 84% on the LIDC–IDRI dataset.

2.4. Lung Cancer Detection Using DL and ML Approach. In order to improve the efficiency of image classification, Bansal et al. [25] proposed an approach that integrates deep features generated with VGG19, a DL model, with other customized feature extraction techniques such as SIFT, SURF, ORB, and the Shi-Tomasi corner detector algorithm. The features were then used in conjunction with various ML algorithms for classification. The empirical findings of the study demon-strated that RF classifier, when combined with the cooperative features extracted using the integrated approach, outper-formed other classifiers with an accuracy of 93.73%. This suggests that utilizing a combination of DL features and clas-sical features yields more consistent and accurate outcomes compared to relying solely on a single feature extractor.

Toğaçar [26] introduced DL model where the image classes were constructed using the DarkNet-19 model as a foundation. To build the image classes, the weak features were selected from the feature set obtained from the Dar-kNet-19 model using the equilibrium and manta-ray forag-ing optimization approach. These weak features were then separated from the rest of the feature set to create an optimal feature set. The support vector machine (SVM) approach was employed to classify the suitable characteristics gener-ated by the two optimization algorithms utilized. The overall performance of the classifier achieved an impressive percent-age of 99.69%. The evaluation results revealed a remarkable area under curve (AUC) value of 99.3%. Furthermore, the technique demonstrated high F-measure, precision, recall, and accuracy rates, with values reaching 97.1%. This DL model developed by Tougaccar showcases the effectiveness of com-bining different optimization algorithms and strategies to enhance the categorization ability of the dataset. The impres-sive performance metrics, including AUC, F-measure, preci-sion, recall, and accuracy, highlight the model's capabilities in accurately classifying images. Second Dritsas and Mesut [27] propose the use ML methods, specifically the rotation forest model, to efficiently identify developing lung cancer.

2.5. Lung Cancer Detection Using Hybrid Approach. Talukder et al. [28] proposed a hybrid ensemble feature extraction model to effectively identify lung cancer. The model was evaluated on lung datasets, specifically the LC25000 dataset. The study findings revealed hybrid model to achieved impressive accuracy rates of 99.05% in detecting lung cancer. These results demonstrate the efficacy of the proposed strat-egy in accurately diagnosing lung cancer. Furthermore, the study showed that the proposed hybrid model outperformed existing models significantly, indicating its potential applica-bility in clinical settings. This demonstrates the effectiveness of using ensemble models of TL models to enhance the effi-ciency of lung cancer diagnosis.

In the study by Phankokkruad [7], three TL models were employed. The results showed that VGG16 achieved an accuracy of 62%, ResNet50V2 achieved 90%, and Dense-Net201 achieved 89%. However, when these models were combined into an ensemble model, the validation accuracy increased to 91%. This demonstrates the effectiveness of using ensemble models of TL models to enhance the effi-ciency of lung cancer diagnosis. Similarly, Chen et al. [10] proposed a hybrid classifying framework for distinguishing lung cancer and normal tissue in the lung pathology images. The framework combined the Inception v3 model with fea-ture extraction modules such as hog and daisy. The experi-mental findings revealed an impressive accuracy of 99.60%, surpassing the results of other comparable trials. These

International Journal For Recent Developments in Science & Technology
2581-4575
Crossref
A Peer Reviewed Research Journal

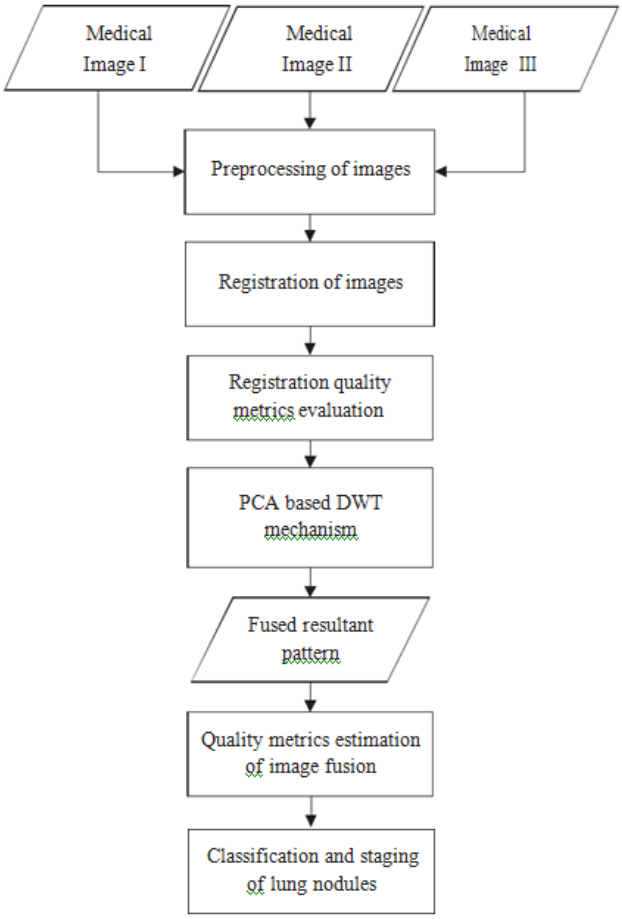

FIGURE 1: Recommended technique's block diagram.

findings highlight the potential of hybrid DL models in pro-viding a reliable approach for cancer diagnosis.

3. Proposed Method

The proposed method for image fusion is based on MRR and DWT-PCAv methods in this study. The MRR method is highly precise compared to SRR. The resulting image is then enhanced with the DWT-PCAv fusion technique. Med-ical CT images are used as input in the current study. The MRR technique is used to line up the images and compare the different levels of their intensities in the initial step of the registration process. It has been noted that the suggested method produces preferable results to the SRR technique. The resulting image is perfectly fitted and provides more useful diagnostic information. The DWT-PCAv fusion method is used to merge both images after registration. Figure 1 depicts the overall proposed method's structure. The resulting image is perfectly lined up and provides useful diagnostic data. The DWT-PCAv fusion method is used to merge multiple images after registration. Figure 2(a) shows the source image and Figure 2(b) shows the enhanced image, which is used in the next process of this study, and Figure 3 depicts the proposed fusion method's structure.

3.1. Multiresolution Rigid Registration (MRR). The improved input medical images are changed at various resolution levels during the MRR process. The multiview registration pyramid is shown in Figure 4. The pyramid's top image has a smaller resolution than its base image.

Each level of the separated images will go through a registration process. The registration procedure will produce better results if the input images are identical in size and resolution, and will aid in diagnosing imperfections. The pyramid's base contains the original input images.

International Journal For Recent Developments in Science & Technology
2581-4575
Crossref
A Peer Reviewed Research Journal

if they are N × N, the following stage would be N=2 × N=2 and N=3 × N=3, the fourth level would be N=4 × N=4. MRR is a geometric transformation iterative process that exploits the similarity between the source and targeted image.

The proposed algorithm presented in Equation (1) offers a multiview similarity measurement between two images with distinct intensity distributions. Let D_1 and D_2 represent the two volume images being compared in terms of their pixel intensities.

In the kth voxel, the mean intensity ðy¯ kÞ is utilized as the comparable value between images D_1 and D_2, while the variance ð σkÞ provides a confidence weight for the cost function in Equation (1,) as introduced by Equation (2).

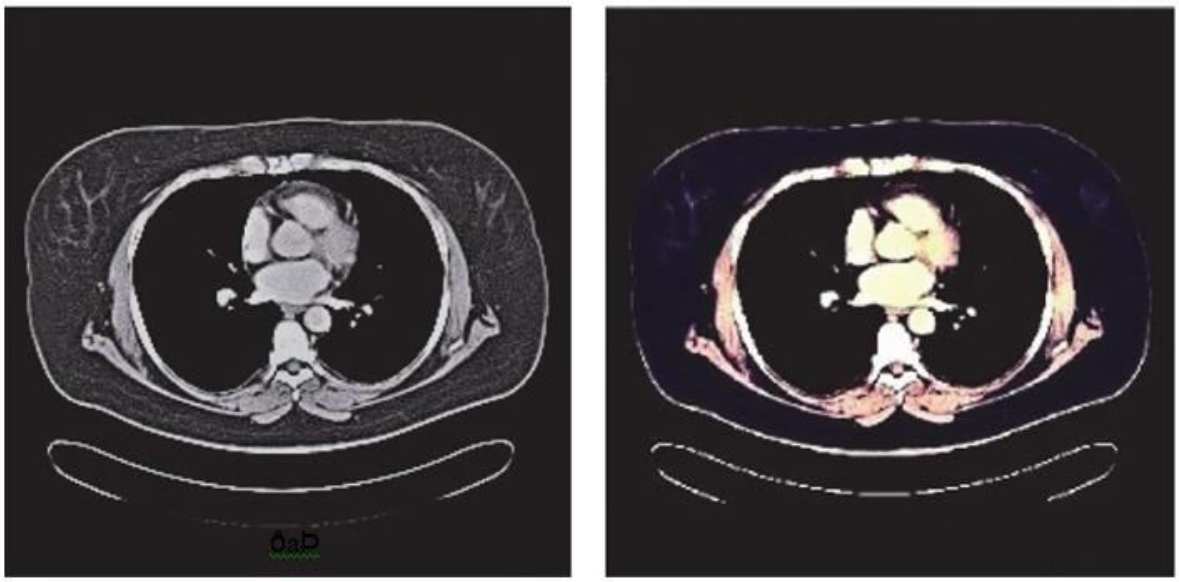

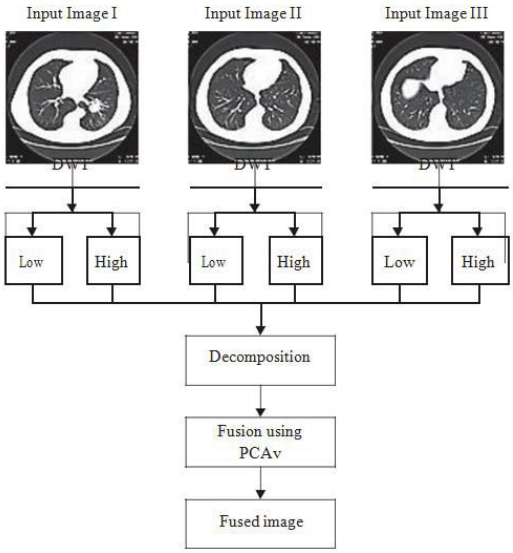

FIGURE 3: DWT-PCAv fusion process.

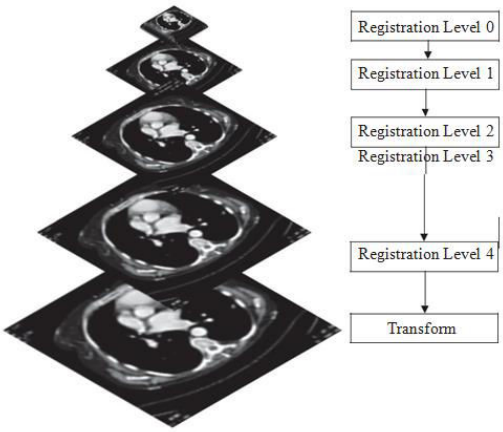

FIGURE 4: Pyramid model of multiview for registration.

a high resolution. Nuclear magnetic resonance technology is used in MRI imaging. While it can collect soft tissue details from the human body, it does so at a lower resolution [14].

Recently, the coronavirus disease (COVID-19) outbreak has spread over the world and become a worldwide threat since the end of 2019, prompting the World Health Organi-zation (WHO) to label the outbreak a pandemic. Nucleic acid testing is currently used to diagnose COVID-19, although it can result in false negatives. Lung CT scans can be used to screen and monitor diagnosed cases more effec-tively. Computer-aided diagnosis (CAD) technologies can relieve doctors of their responsibilities, allowing for more quick and more large -scale diagnostic screening. Image fusion, medical image processing technologies, and com-puter analysis are used in the CAD system.

To identify and classify lung cancer efficiently, this study introduces a methodology for designing an effective ML-classification model. The model is specifically designed to extract crucial information from medical images while con-serving image energy. Furthermore, this study presents novel algorithms for multiview medical image registration and fusion, specifically applied to CT scans. To accomplish this, it is crucial to train our model using a large dataset that encompasses all possible instances of cancer. As a result, our research focuses on application of a comprehensive and well-organized dataset called LIDC–IDRI (lungs image database consortium–image database resource initiative) on our proposed technique. Additionally, several preprocessing methods are applied to the datasets to enhance their quality. In order to enhance the robustness and accuracy of our model, we incorporate k-fold cross-validation during the training process. This technique allows for comprehensive validation and assessment of the model's performance. More-over, we apply feature extraction techniques on the dataset to extract valuable information that is crucial for effective model training. To further improve the performance of cancer clas-sification, we employ an ReNet 18 model in our implementa-tions. By using this model, we are able to achieve enhanced predictive capabilities and overall better performance in clas-sifying cancer cases. This approach ensures a more robust and reliable model for accurate cancer diagnosis.

In this study, the performance of our proposed model relies on the effective utilization of a multilayer convolutional neural network (CNN). The ReNet 18 model is specifically designed to identify the tumors accurately and classify their respective stages. This model demonstrates promising results in accurately diagnosing and classifying tumors based on their stage. During the evaluation of our models, we considered several performance indicators to assess their effectiveness. These indicators include precision, recall, accuracy, mutual information (MI), normalized cross-correlation (NCC), peak signal-to-noise ratio (PSNR), and root-mean-square error (RMSE). By analyzing the models from various aspects and considering the classifier algorithm employed in the proposed model, we achieved a high-accuracy rate 98.2% in the detec-tion of lung cancer. Therefore, the main proposition of this research paper is to propose and demonstrate the effective-ness of a novel approach in detecting and classifying lung

3.2. DWT-PCAv Fusion. Following the MRR approach, the input source images are divided into distinct multiview reso-lutions and rotations utilizing DWT.

Figure 3 shows the entire step-by-step fusion process. This procedure is utilized to view input images at various levels, with each deconstructed level holding unique data. After the multiscale breakdown, the main elements are com-puted on every image coefficients level. On each level of a decomposed image, the mean of the key elements is calcu-lated, and weights are given to each image coefficient variable for fusion rules. High–high (HH), high–low (HL), low–high (LH), and low–low (LL) coefficient levels are applied to the input images.

The detailed coefficient scale levels LH, HL, and HH are present, while the approximate coefficients factor LL is also presented. The PCA is fed with the LL coefficient compo-nents from two source images. The new coefficient elements n_1, n_2, and n_3 are determined from the LL coefficients com-ponents. To measure the principle components, other com-plete coefficient components are also managed. The average of the key elements of the estimation and coefficients is then used to calculate the n_1, n_2, and n_3 average components. Finally, the final image is fuzed using these two average principal components.

The following are the key steps:

(1) In the beginning, DWT is used to decompose CT input images into two or three stages.

(2) After that, PCA is used to obtain detailed coefficients and approximation components.

(3) Multiple multiview source images classify each prin-ciple element of corresponding coefficient elements.

(4) PCAv technique is used to determine the average coefficient components.

(5) Using the mean and averaging principal components to implement the PCAv fusion approach.

(6) Diagonal matrix can be define as E which contains the eigenvalues. p denotes the decomposition levels. n_1, n_2, and n_3 are determined from estimation coefficients, elements in the following equations. After calculating all of the n_1, n_2, and n_3 components, the average of these elements is calcu-lated from the

International Journal For Recent Developments in Science & Technology
2581-4575
Crossref
A Peer Reviewed Research Journal

given below equations. The final medical image is fuzed using the PCAv with valuable assessment details in the final stage.

3.3.1. Lung Nodule Segmentation. Lung nodule segmentation was an important step in the detection of nodules. In order to achieve this, we implemented optimal thresholding which was followed by contour correction and labeling of the con-nected components. The following steps were adopted for the lung nodule segmentation:

Initially, the lung volume was evaluated by using the com-ponent labeling approach after the fuzed CT images have been segmented using optimal thresholding.

To achieve optimal thresholding, we denote the thresh-old after the nth step as T_n. The lung CT scan can be cate-gorized into two density groups. The HU values in the lung CT scan typically range from −2,000 to +2,000 HU. The low-density area, known as the lung area or nonbody area, encompasses HU values ranging from −1,000 to −500 HU. The nonbody area, which includes the CT-scanner area, is distinct from the body area that encompasses the surround-ings of the lung lobes. Since the lungs are situated within the nonbody area, an initial threshold value −500 HU (denoted as T_o) is selected. To determine the new threshold, we apply T_n to the lung image. Let ϵ_{oj} and ϵ_{bg} represent the mean

In which a and b indices represent the slice coordi-nates and c indicates the slice number with each individ-ual slice has dimensions of a × b pixel.

(2) After applying optimal threshold we obtained a lung CT image having a body and nonbody areas after applying the optimal thresholding. Black belongs to the body area, whereas white belongs to the nonbody area. The first and second biggest lung volumes were identified using connected component labeling on a thresholded image. The majority of the undesirable nonbody areas were ignored while choosing the volume.

(3) The final image after background removal has holes in the lung lobes that might contain prospective nodules. Morphological operations were used to fill the holes for the accurate detection of nodules.

(4) Finally, the rolling ball algorithm was used to smooth the lung juxta pleural nodes.

3.3.2. Extraction of Nodule Candidates. There were deter-mined to be three different kinds of lung nodules: isolated, juxta-pleural, and juxta-vascular. By using the suggested approach, there were further substeps involved for the extrac-tion of lung nodules. In the first step, improved Ostu's method was used for grouping and labeling lung nodules. After that dot-shape selective enhancement filter was used to distinguish the spherical, tubular, and planner structure of nodules. The optimal thresholding was used to detect the nodules. Finally, a rule-based analysis has been performed to select whether to keep or discard the detected nodule based on area, volume, and diameter. A nodule candidate with a volume of more than 30 mm should be recognized as a mass or nonnodule since nodules range in size from 3 to 30 mm. Following rule-based analysis, many features from prospective nodule candidates were selected and applied to train the GA-CNN classifier.

3.3.3. Stage Classification of Lung Nodule. Final resultant fuzed lung nodule images were used as input in our proposed ResNet-18 multilayer method. ResNet-18 is a CNN

TABLE 1: Classification of lung cancer stages based on size.

Cancer stage	Size of nodules
STG-1	3–10 mm
STG-2	>10–<15 mm
STG-3	≥15–<25 mm
STG-4	≥25 mm

International Journal For Recent Developments in Science & Technology
2581-4575
Crossref
A Peer Reviewed Research Journal

TABLE 2: ResNet-18 structuural detail.

S. no	Input image			Output image			Layers	Stride	Kernal	
1	227	227	3	112	112	64	Conv 1	2	7	7
	112	112	64	56	56	64	Max pool	2	3	3
2	56	56	64	56	56	64	Conv 2-1	1	3	3
3	56	56	64	56	56	64	Conv 2-2	1	3	3
4	56	56	64	56	56	64	Conv 2-3	1	3	3
5	56	56	64	56	56	64	Conv 2-4	1	3	3
6	56	56	64	28	28	128	Conv 3-1	2	3	3
7	28	28	128	28	28	128	Conv 3-2	1	3	3
8	28	28	128	28	28	128	Conv 3-3	1	3	3
9	28	28	128	28	28	128	Conv 3-4	1	3	3
10	28	28	128	14	14	256	Conv 4-1	2	3	3
11	14	14	256	14	14	256	Conv 4-2	1	3	3
12	14	14	256	14	14	256	Conv 4-3	1	3	3
13	14	14	256	14	14	256	Conv 4-4	1	3	3
14	14	14	256	7	7	512	Conv 5-1	2	3	3
15	7	77	512	7	7	512	Conv 5-2	1	3	3
16	7	7	512	7	7	512	Conv 5-3	1	3	3
17	7	7	512	7	7	512	Conv 5-4	1	3	3
	7	7	512	1	1	512	Avg-pool	7	7	7
18	1	1	512	1	1	1,000	fc			

TABLE 3: Performance metrics for 10-fold cross-validation.

K-Fold	Precision (%)	Recall (%)	Accuracy (%)
Onefold	97.5	96.4	96.5
Twofold	98.7	98.1	99.5
Threefold	99.3	97.3	99.7
Fourfold	97.4	96.4	96.3
Fivefold	99.2	97.7	99.6
Sixfold	99.7	96.2	96.1
Sevenfold	97.8	97.6	98.1
Eightfold	97.9	97.4	99.6
Ninefold	97.1	97.4	98.6
Tenfold	98.6	98.3	98.0
Mean value	98.32	97.28	98.20

architecture that consists of 18 layers. The network is divided into four identical ConvNets layers. Each layer is composed of two residual blocks. Each block contains two weight layers, and the output of the second weight layer is connected to the input using a skip connection with a rectified linear unit (ReLU) activation. The network incorporates two pooling layers, one at the start (max pooling) and another at the end (global average pooling). The ResNet-18 architecture takes an input size of 227, 227, 3, where 227 represents the width and height of the input image, and 3 represents the RGB channels with 0.2 dropout and 8,192 units of fully connected layer used to classify and achieve the 98.2% accu-racy in the classification of lung cancer stage. Table 1 repre-sents the classification of lung cancer based on nodule size.

Table 2 represents the output of ResNet-18 is passed through a fully connected (FC) layer, which then serves as input to the sequential layer for further processing or classi-fication tasks. The suggested model was used to investigate the kernel. The first layer and average pooling layers have a 7 × 7 kernel while the remaining layers have a 3 × 3 kernel whose function is to categorize the stages of lung tumors. We trained our proposed model in each of the 30 epochs. By using the factor value of 10 epochs, the learning rate μ in

International Journal For Recent Developments in Science & Technology
2581-4575
Crossref
A Peer Reviewed Research Journal

TABLE 3: Performance metrics for 10-fold cross-validation.

K-Fold	Precision (%)	Recall (%)	Accuracy (%)
Onefold	97.5	96.4	96.5
Twofold	98.7	98.1	99.5
Threefold	99.3	97.3	99.7
Fourfold	97.4	96.4	96.3
Fivefold	99.2	97.7	99.6
Sixfold	99.7	96.2	96.1
Sevenfold	97.8	97.6	98.1
Eightfold	97.9	97.4	99.6
Ninefold	97.1	97.4	98.6
Tenfold	98.6	98.3	98.0
Mean value	98.32	97.28	98.20

each of the 8 epochs was reduced using the proposed model. Therefore, our proposed model achieved accuracy to predict the early cancer stage

The main purpose of adding global average pooling to the base model (ResNet-18) is to prepare the model for the final classification layer. This calculates the average output of each feature map from the preceding layer, resulting in a global representation of the entire feature map. This pooling operation reduces the spatial dimensions of the feature maps to a single value per channel. One of the key benefits of using the model is its ability to help stabilize validation accuracy, which serves as an indicator of over fitting. By aggregating spatial information into a single value per channel, global average pooling reduces the risk of over fitting by preventing the model from excessively focusing on specific spatial locations. In addition, it also contributes to reducing the compu-tation time of the CNN model. By adding fully connected layers with a global pooling layer, the number of parameters to be learned and the overall computational complexity of the model is significantly reduced.

3.3.4. Cross-Validation Set. In this proposed method, the tenfold cross-validation approach was used. Nine sets were utilized for training and one set was used for validation with a repeat of 15 epochs in the tenfold cross-validation set. There will be 150 epochs in total for the training operations with a batch size of 10. For the cross-validation set, we fold our dataset into a set of images that is tenfolds. Using the same dataset of images, we examined folds 1, 4, and 6, and the findings were less accurate than those of the other fold sets. The accuracy, precision, and recall performance metrics for tenfold cross-validation with the mean value are shown in Table 3.

4. Results

For the evaluation of the proposed technique, the LIDC dataset is used for our proposed methodology, which has DICOM image format [29]. In Section 4.1 LIDC dataset will be discussed in detail. The performance parameters dis-cussed are used for the evaluation of the proposed technique. The results of the proposed technique are presented and also compared with the results of other techniques in detail. The
environment for the experimental work was MATLAB 2016a and Dell Latitude E6230 which has 16 GB of RAM. More-over, this machine runs on an Intel Core i5 processor (CPU capacity is 2.70 GHz).

4.1. Imaging Database. The LIDC is commonly used to evalu-ate proposed techniques as revealed in the literature review. LIDC is hosted by the cancer imaging archive (CIA) which has provided LIDC on their website of TCIA [30] without any cost.

This dataset comprises of 4,682 CT-scan images of 61 patients of lung cancer, which include nodules ranging in size from 3 to 30 mm that four expert radiologists annotated in two sessions. Each patient has 60–120 slices, each of which is 512 × 512 pixels in size and has 4,096 gray levels in HU. About 0.78–1 mm is the range of pixel spacing, with a 1–3 mm reconstruction interval.

4.2. Performance Parameters. The proposed model is vali-dated using the metrics like MI, feature mutual information (FMI), NCC, RMSE, structural similarity index metric (SSIM), and PSNR. MI decides how information from source images and fuzed images are combined [31]. If the resultant image and source image does not depend on each other then the MI will be zero [32]. More information is common between the resul-tant image and source image if the MI is higher. MI can be expressed by Zhang et al. [33] as follows:

International Journal For Recent Developments in Science & Technology
2581-4575
Crossref
A Peer Reviewed Research Journal

$$MI_{xy} = G_x + G_y - G_{xy}; \quad (20a)$$

$$MI_O = MI_{OX} + MI_{Oy}; \quad (20b)$$

where G_x indicates the joint entropy of image X and G_y means the joint entropy of image Y, and G_{xy} denotes the joint entropy of image X and Y. MI_{xy} signifies the mutual knowledge between the source and the consequent image. Similar to this, Equation (20b) defines MI of the fuzed image, which is MI_O. PSNR is an RMSE-based quantitative measure. PSNR calculates the ratio of intensity levels in medical images to the corresponding pixels in the final image. A higher PSNR value indicates higher quality fusion or registration.

$$PSNR = 10 \times \log_{10} \frac{(f_{max})^2}{RMSE} : \quad (21)$$

The highest pixel gray levels quantity in the fuzed image is indicated by f_{max}. The SSIM estimates the similarity among two regions z_x and z_y in images X and Y. Where z_x and z_y are the local means, $\sigma z_x z_y$ is the standard deviation, h_1 and h_2 are the positive constants.

4.3. Outcomes of MRR. Figure 2 shows the preprocessed enhanced image. After preprocessing, registration is the most crucial step. Registration affects fusion efficiency as well. Intensity-based registration works well with multiview image registration. Both rigid registration techniques are applied to CT-lung images. These approaches were chosen because full image alignment can be completed rapidly, whereas time complexity is not an issue in SRR. But, the quality of image registration is compromised.

Lung registered images' visual outcomes having a definite deviation are demonstrated to evaluate improved registra-tion outcomes. Evidence shows that these outcomes suit human perception. Figure 5 shows the results of MRR tech-nique implemented on different lung CT images of patients. Each set of CT images is divided into three parts from (a to i), the "left" side shows the source image, the "center" side shows the thick boundary identification, and the "right" side shows the resultant images after applying the MRR technique while Table 4 represents the results of image reg-istration quality assessments measures. Furthermore, statis-tical analyses are performed to show which technique produces significant results in the registration process. In most circumstances, the MRR performs better. RMSE, NCC, SSIM, PSNR, CC, SSD, and MI are the seven registra-tion quality assessment measures that have been chosen for validation. Both registration methods' computing costs are also computed.

For better image registration, we need high values of PSNR, CC, NCC, SSIM, and MI, while the values of SSD and RMSE should be low. Table 4 displays the statistical results of lung image registration.

Figure 6(a)–6(e) show the experimental results for the different patients of lung CT images. The approach used to create these lung image registrations with various SRR per-formance factors. All images are slightly blurred with a lot of noise, color distortion, and low contrast and do not contain all the required information found in the original

International Journal For Recent Developments in Science & Technology
2581-4575
Crossref
A Peer Reviewed Research Journal

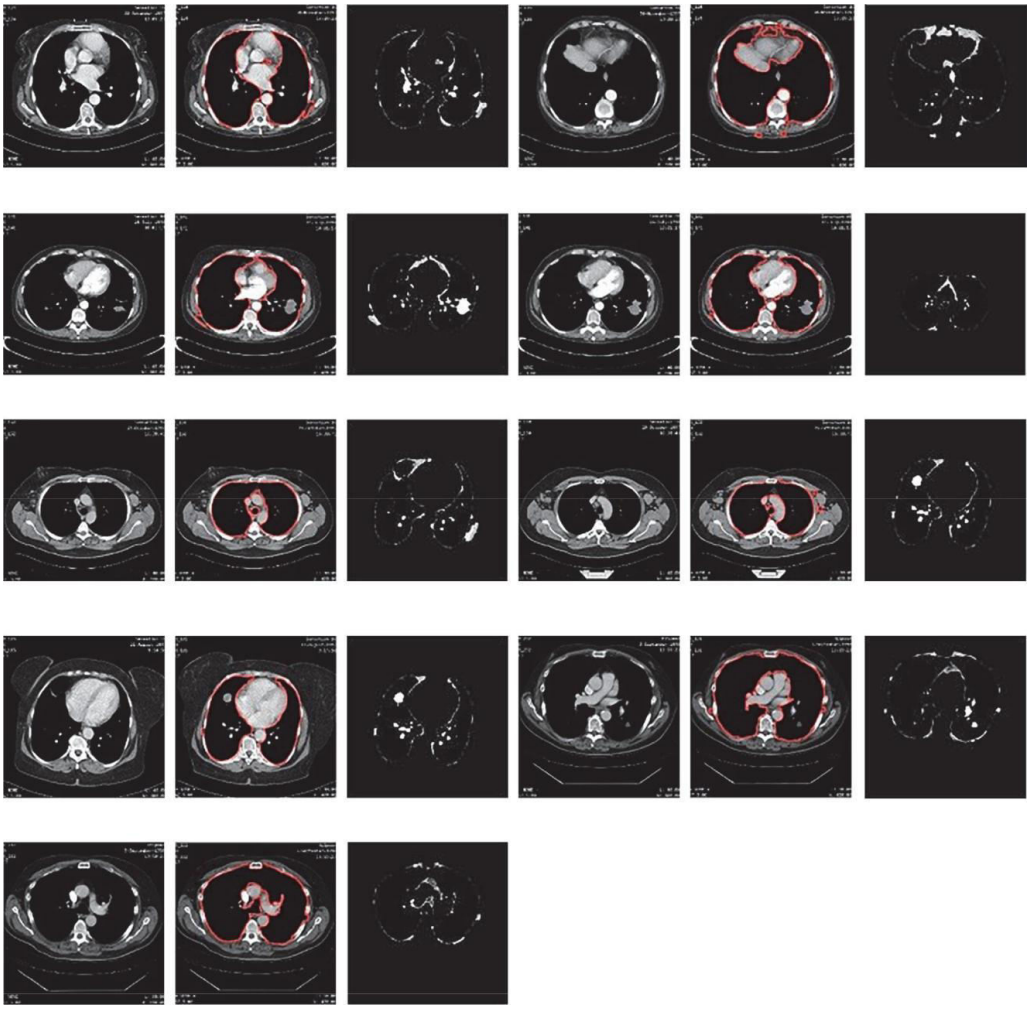

5. Discussion

ML has undoubtedly emerged as a crucial tool for healthcare professionals and clinicians, particularly in early diagnosis of lung cancer. To achieve the desired level of precision and accuracy, numerous algorithms have been proposed. In light of this, a novel method utilizing the ResNet-18 CNN approach has been applied. This method incorporates the application of DWT and PCAv techniques. By leveraging these techniques and considerations, the aim is to enhance the overall performance and reliability of the diagnosis pro-cess. Multiview image registration involves merging infor-mation from multiple images to enhance the precision of analysis. Aligning these images is crucial to extract meaning-ful and reliable information. Furthermore, if one of the images contains its corresponding segmentation, the labeled image can be transformed using the same alignment techni-ques applied to synchronize it with the reference image. Our proposed method MRR has been extensively compared to various approaches presented in other research papers, and

6. Conclusion and Impending Work

The paper introduces a novel approach for the detection and classification of lung cancer. This model integrates various components including preprocessing techniques, k-fold cross-validation (with a fold size of 10), and feature extrac-tion using ResNet-18 model. Simultaneously, to assess the performance of the system using ML algorithms, the study

employed six widely used algorithms: $L_{AB=F}^{A}$, $N_{AB}^{m}{}_{=F}$, $Q_{TEIAB=F}$, Q, Q, and VIF. To evaluate the comprehensive development, a range of performance metrics has been employed, including accuracy, recall, precision, RMSE, FMI, CC, NCC, SSIM, PSNR, and MIF. In our experiment, we utilized the LIDC–IDRI image datasets and found that our model demonstrates best performance in diagnosing lung cancer. Compared to classification methods, the pro-posed methodology for image registration and fusion intends to decrease the number of physical checks while increasing the precision of the auto procedure. The proposed MRR eliminates the SRR's drawback. The SRR is a time-saving method, but it comes with the risk of registration. The fusion phase uses the MRR-recorded image as an input. By fuzing three lung images thus preserving important details, the PCAv fusion technique enhances the image quality. PCAv fusion also has the benefit of being time-saving. The sug-gested technique is applied to the whole dataset of lung images, one of which contains regular source images, the second contains the segmented images, and the last one is the final resultant fuzed images. Established fusion approaches are contrasted with the proposed approach. Visual and statis-tical representations of the image registration and fusion results are given. Moreover, the suggested ResNet-18 model for nodule classification was applied to unsupervised learning neural networks as a stage classifier and predictor to detect nodules more accurately. The accuracy, sensitivity, and speci-ficity of the performance metrics were also calculated and compared with the existing approaches. The findings indicate that stage categorization for evaluated segmented fuzed images was 98.2% accurate. In comparison to other existing techni-ques, the proposed approach shows potential. Researchers will continue to work on nonrigid registration in this field and apply their findings to other image modalities procedures. For improved results, this study may be integrated with ML models, such as the quick and portable 3D CNN. The cutting-edge research can be applied to a variety of current diseases including COVID-19 and its effects on lung psychology.

References

[1] G. Qu, D. Zhang, and P. Yan, "Medical image fusion by wavelet transform modulus maxima," Optics Express, vol. 9, no. 4, pp. 184–190, 2001.
[2] R. Tekade, "Lung nodule detection and classification using machine learning techniques," Asian Journal for Convergence in Technology, vol. 4, 2018.
[3] W.-J. Choi and T.-S. Choi, "Automated pulmonary nodule detection based on three-dimensional shape-based feature descriptor," Computer Methods and Programs in Biomedicine, vol. 113, no. 1, pp. 37–54, 2014.
[4] I. R. S. Valente, P. C. Cortez, E. C. Neto, J. M. Soares, V. H. C. de Albuquerque, and J. M. R. S. Tavares, "Automatic 3D pulmonary nodule detection in CT images: a survey," Computer Methods and Programs in Biomedicine, vol. 124, pp. 91–107, 2016.
[5] L. Hussain, M. S. Almaraashi, W. Aziz, N. Habib, and S. U. R. Saif Abbasi, "Machine learning-based lungs cancer detection using reconstruction independent component analysis and sparse filter features," Waves in Random and Complex Media, pp. 1–26, 2021.
[6] T. V. Pyrkov, K. Slipensky, M. Barg et al., "Extracting biological age from biomedical data via deep learning: too much of a good thing?" Scientific Reports, vol. 8, no. 1, pp. 1–11, 2018.
[7] M. Phankokkruad, "Ensemble transfer learning for lung cancer detection," in 2021 4th International Conference on Data Science and Information Technology, pp. 438–442, Associa-tion for Computing Machinery, 2021.
[8] A. Onan, "On the performance of ensemble learning for automated diagnosis of breast cancer," in Artificial Intelligence Perspectives and Applications: Proceedings of the 4th Computer Science On-Line Conference 2015 (CSOC2015), Vol 1: Artificial Intelligence Perspectives and Applications, pp. 119–129, Springer, 2015.
[9] M. Liang, Z. Ren, J. Yang, W. Feng, and B. Li, "Identification of colon cancer using multi-scale feature fusion convolutional neural network based on shearlet transform," IEEE Access, vol. 8, pp. 208969–208977, 2020.
[10] M. Chen, S. Huang, Z. Huang, and Z. Zhang, "Detection of lung cancer from pathological images using CNN model," in 2021 IEEE International Conference on Computer Science, Electronic Information Engineering and Intelligent Control Technology (CEI), pp. 352–358, IEEE, 2021.
[11] T. R. Mim, M. Amatullah, S. Afreen et al., "GRU–INC: an inception–attention based approach using GRU for human activity recognition," Expert Systems with Applications, vol. 216, Article ID 119419, 2023.
[12] D. A. Palanivel, S. Natarajan, and S. Gopalakrishnan, "Muti-fractals based multimodal 3D image registration," Biomedical Signal Processing and Control, vol. 47, pp. 126–136, 2019.
[13] Z. Cui, S. Mahmoodi, M. Guy et al., "A general framework in single and multi-modality registration for lung imaging analysis using statistical prior shapes," Computer Methods and Programs in Biomedicine, vol. 187, Article ID 105232, 2020.
[14] R. Bashir, R. Junejo, N. N. Qadri, M. Fleury, and M. Y. Qadri, "SWT and PCA image fusion methods for multi-modal imagery," Multimedia Tools and Applications, vol. 78, no. 2, pp. 1235– 1263, 2019.
[15] F. Silva, T. Pereira, I. Neves et al., "Towards machine learning-aided lung cancer clinical routines: approaches and open challenges," Journal of Personalized Medicine, vol. 12, no. 3, Article ID 480, 2022.
[16] A. A. Alsheikhy, Y. Said, T. Shawly, A. K. Alzahrani, and

H. Lahza, "A CAD system for lung cancer detection using hybrid deep learning techniques," Diagnostics, vol. 13, no. 6, Article ID 1174, 2023.
[17] X. Li and J. Zhao, "A novel multi-modal medical image fusion algorithm," Journal of Ambient Intelligence and Humanized Computing, vol. 12, no. 2, pp. 1995–2002, 2021.
[18] J. R. Benjamin and T. Jayasree, "Improved medical image fusion based on cascaded PCA and shift invariant wavelet transforms," International Journal of Computer Assisted Radiology and Surgery, vol. 13, no. 2, pp. 229–240, 2018.
[19] N. Aishwarya and C. Bennila Thangammal, "A novel multimodal medical image fusion using sparse representation and modified spatial frequency," International Journal of Imaging Systems and Technology, vol. 28, no. 3, pp. 175–185, 2018.
[20] N. Faruqui, M. A. Yousuf, M. Whaiduzzaman, A. K. M. Azad,
A. Barros, and M. A. Moni, "LungNet: a hybrid deep-CNN model for lung cancer diagnosis using CT and wearable sensor-based medical IoT data," Computers in Biology and Medicine, vol. 139, Article ID 104961, 2021.
[21] I. M. Nasser and S. S. Abu-Naser, "Lung cancer detection using artificial neural network," International Journal of Engineering and Information Systems, vol. 3, pp. 17–23, 2019.
[22] A. Shimazaki, D. Ueda, A. Choppin et al., "Deep learning-based algorithm for lung cancer detection on chest radiographs using the segmentation method," Scientific Reports, vol. 12, no. 1, Article ID 727, 2022.
[23] M. R. Hasan and M. Al Kabir, "Lung cancer detection and classification based on image processing and statistical learning," Journal of Emerging Trends in Engineering and Applied Sciences, vol. 11, pp. 229–236, 2020.
[24] S. Bhatia, Y. Sinha, and L. Goel, "Lung cancer detection: a deep learning approach," in Soft Computing for Problem Solving: SocProS 2017, vol. 2, pp. 699–705, Springer, 2019.
[25] M. Bansal, M. Kumar, M. Sachdeva, and A. Mittal, "Transfer learning for image classification using VGG19: Caltech-101 image data set," Journal of Ambient Intelligence and Humanized Computing, vol. 14, no. 4, pp. 3609–3620, 2023.
[26] M. Toğaçar, "Disease type detection in lung and colon cancer images using the complement approach of inefficient sets," Computers in Biology and Medicine, vol. 137, Article ID 104827, 2021.
[27] E. Dritsas and M. Trigka, "Lung cancer risk prediction with machine learning models," Big Data and Cognitive Computing, vol. 6, no. 4, Article ID 139, 2022.
[28] M. A. Talukder, M. M. Islam, M. A. Uddin, A. Akhter,
K. F. Hasan, and M. A. Moni, "Machine learning-based lung and colon cancer detection using deep feature extraction and ensemble learning," Expert Systems with Applications, vol. 205, Article ID 117695, 2022.
[29] S. G. Armato III, G. McLennan, M. F. McNitt-Gray et al., "Lung image database consortium: developing a resource for the medical imaging research community," Radiology, vol. 232, no. 3, pp. 739–748, 2004.
[30] K. Clark, B. Vendt, K. Smith et al., "The Cancer Imaging Archive (TCIA): maintaining and operating a public informa-tion repository," Journal of Digital Imaging, vol. 26, no. 6, pp. 1045–1057, 2013.
[31] F. Maes, D. Vandermeulen, and P. Suetens, "Medical image registration using mutual information," Proceedings of the IEEE, vol. 91, no. 10, pp. 1699–1722, 2003.
[32] S. D. Ramlal, J. Sachdeva, C. K. Ahuja, and N. Khandelwal, "An improved multimodal medical image fusion scheme based on hybrid combination of nonsubsampled contourlet transform and stationary wavelet transform," International Journal of Imaging Systems and Technology, vol. 29, no. 2, pp. 146–160, 2019.
[33] X. L. Zhang, Z. F. Liu, Y. Kou, J. B. Dai, and Z. M. Cheng, "Quality assessment of image fusion based on image content and structural similarity," in 2010 2nd International Conferenceon Information Engineering and Computer Science, pp. 1–4, IEEE, 2010.
[34] K. Zhan, Y. Xie, H. Wang, and Y. Min, "Fast filtering image fusion," Journal of Electronic Imaging, vol. 26, no. 6, Article ID 063004, 2017.
[35] D. P. Bavirisetti, V. Kollu, X. Gang, and R. Dhuli, "Fusion of MRI and CT images using guided image filter and image statistics," International Journal of Imaging Systems and Technology, vol. 27, no. 3, pp. 227–237, 2017.
[36] R. Vijayarajan and S. Muttan, "Discrete wavelet transform based principal component averaging fusion for medical images," AEU—International Journal of Electronics and Communications, vol. 69, no. 6, pp. 896–902, 2015.
[37] Z. Liu, E. Blasch, Z. Xue, J. Zhao, R. Laganiere, and W. Wu, "Objective assessment of multiresolution image fusion algorithms for context enhancement in night vision: a comparative study," IEEE Transactions on Pattern Analysis and Machine Intelligence, vol. 34, no. 1, pp. 94–109, 2012.
[38] C. Yang, J.-Q. Zhang, X.-R. Wang, and X. Liu, "A novel similarity based quality metric for image fusion," Information Fusion, vol. 9, no. 2, pp. 156–160, 2008.
[39] Z. Zhu, G. Qi, Y. Chai, H. Yin, and J. Sun, "A novel visible–infrared image fusion framework for smart city," International Journal of Simulation and Process Modelling, vol. 13, no. 2, pp. 144–155, 2018.
[40] H. R. Sheikh and A. C. Bovik, "Image information and visual quality," IEEE Transactions on Image Processing, vol. 15, no. 2,
pp. 430–444, 2006.
[41] V. Petrovic and C. Xydeas, "Objective image fusion performance characterisation," in Tenth IEEE International Conference on Computer Vision (ICCV'05) vol. 1, vol. 2,
pp. 1866–1871, IEEE, 2005.
[42] I. Nazir, I. U. Haq, M. M. Khan, M. B. Qureshi, H. Ullah, and S. Butt, "Efficient pre-processing and segmentation for lung cancer detection using fused CT images," Electronics, vol. 11, no. 1, Article ID 34, 2022.

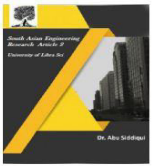

[43] E. S. Neal Joshua, D. Bhattacharyya, M. Chakkravarthy, and Y. C. Byun, "3D CNN with visual insights for early detection of lung cancer using gradient-weighted class activation," Journal of Healthcare Engineering, vol. 2021, Article ID 6695518, 11 pages, 2021.

[44] S. M. Naqi, M. Sharif, and A. Jaffar, "Lung nodule detection and classification based on geometric fit in parametric form and deep learning," Neural Computing and Applications, vol. 32, no. 9, pp. 4629–4647, 2020.

[45] G. Kasinathan and S. Jayakumar, "Cloud-based lung tumor detection and stage classification using deep learning techniques," BioMed Research International, vol. 2022, Article ID 4185835, 17 pages, 2022.

[46] H. Xie, D. Yang, N. Sun, Z. Chen, and Y. Zhang, "Automated pulmonary nodule detection in CT images using deep convolutional neural networks," Pattern Recognition, vol. 85,
pp. 109–119, 2019.

[47] F. Shaukat, G. Raja, R. Ashraf, S. Khalid, M. Ahmad, and A. Ali, "Artificial neural network based classification of lung nodules in CT images using intensity, shape and texture features," Journal of Ambient Intelligence and Humanized Computing, vol. 10, no. 10, pp. 4135–4149, 2019.